

Temperature Sensor Comparison Study of Spot Pyrometers and Contact Thermocouples for Improved Thermal Monitoring of Wire-Arc DED

Charlotte Thompson^{1,2}, Reid Schaff^{1,2}, J. Logan Betts², Matthew W. Priddy^{1,2}

¹Michael W. Hall School of Mechanical Engineering, Mississippi State University, Mississippi State, 39762, MS, USA

²Center for Advanced Vehicular Systems, Mississippi State University, Starkville, 39759, MS, USA

Abstract

In arc-DED research, thermocouples are commonly used to measure temperature on the substrate surface and deposited surfaces, while pyrometers are typically used for instantaneous interlayer temperature measurements for interpass temperature estimation. However, the potential of spot pyrometers to serve as an alternative to K-type thermocouples for analyzing thermal histories has not been thoroughly explored. While thermocouples are most accepted for thermal monitoring at a fixed location, their measurements are highly dependent on setup, and they can be time-consuming to install. In contrast, non-contact methods such as spot pyrometers offer faster, simpler integration with greater flexibility. This makes pyrometers a viable option for routine builds as they can be installed once and require minimal adjustments. This study evaluates the feasibility of using spot pyrometers to capture thermal history by comparing their measurements with various thermocouple configurations across different geometries produced using arc-DED with ER70S-6 wire and cold metal transfer (CMT). Data is collected in a synchronized, interoperable format using a previously developed in-situ monitoring framework built on Robot Operating System 2 (ROS 2).

Introduction

Wire-arc directed energy deposition (arc-DED) is a metal additive manufacturing process that leverages robotic welding to fabricate medium- and large-scale parts in a layer-by-layer fashion. This process is a viable alternative to traditional manufacturing methods due to its reduced material waste, cost-effectiveness, short lead times, and design flexibility [1]. However, due to the inherent layer-by-layer nature of this process, arc-DED introduces a complex thermal history, which yields an inhomogeneous microstructure and poses a challenge to achieve desired mechanical properties of deposited parts [2][3][4][5]. Researchers have used temperature sensors in various ways to monitor and quantify this thermal history with the goal of improving the homogeneity of deposited parts by analyzing heat accumulation and cooling rates [6][7]. To enable thermal monitoring of arc-DED, a variety of temperature sensors have been used such as welded thermocouples, probe thermocouples, and single- and multi- wavelength pyrometers [8].

Thermocouples are the most commonly used temperature sensors in arc-DED for thermal monitoring. These sensors allow for direct connection to the surface, which offers more accurate measurement. Because of this, contact thermocouples are considered standard for temperature measurement. They are also popular due to their cost-effectiveness, high temperature sensing ranges, and durability in the welding environment. Thermocouples are most commonly used to evaluate the thermal gradient of a part or validate simulation and infrared (IR) data [9][10]. In current experimental research, they are often spot-welded onto the substrate to evaluate these gradients [11][12]. However, welded thermocouples are limited to sensing areas they can be physically attached to. Therefore, they cannot monitor an active weld pool and must be attached after deposition to observe the gradient over the part and not only on the substrate [13] [14]. This can make working with contact thermocouples a challenge when evaluating the temperature gradient of an actively built part over time, as the setup time required to attach a thermocouple during a build will affect part cooling rates and overall quality. Thermocouples require a significant amount of time to set up depending on the attachment method. The most common method, spot welding them onto the surface with a thermocouple welder, can take multiple hours to complete before starting a build.

Unlike welded thermocouples, pyrometers allow for temperature measurement without a direct connection to the area of interest. These sensors operate by detecting the IR radiation emitted by an object and converting it into an electrical signal – accuracy depends on the emissivity of the target material [15][16]. Pyrometers can be positioned to focus on a single spot or area of interest and may collect data from any location on a deposited part during a build based on how they are set up prior to deposition. Compared to contact thermocouples, pyrometers only require proper mounting equipment and placement, which significantly reduces time since they do not need to be welded onto the surface. In arc-DED, pyrometers are often used to measure the temperature of the part following the melt pool to determine interpass temperature [17][18][19]. They have also been used to monitor thermal cycles and temperature distribution alongside thermocouples in a few studies [13][20][21]. This study aims to compare data collected with 1D spot pyrometers and K-type contact thermocouples to determine the efficacy of using a spot pyrometer in place of K-type contact thermocouples for monitoring the temperature evolution of a part during deposition.

Methodology

Three types of temperature sensors were used to compare thermal monitoring: welded K-type thermocouples, probe K-type thermocouples, and non-contact 1D spot pyrometers. The welded K-type thermocouples were made from K-type wire by creating a junction between the hot and cold ends to create voltage potential that can be converted to a temperature value. These K-type thermocouples can provide measurements from -200 to 1250 °C through direct contact and have an operating temperature range of up to 700 °C with their fiberglass braided jacket. The contact probe K-type thermocouple allows for measurements of 0 °C to 1038 °C. The 1D

(single-color) spot pyrometers used are Optris CS LT IR pyrometers with a distance-to-spot-size ratio of 15:1, a temperature range of -50 to 1030 °C, and an operating temperature up to 80 °C. These pyrometers have a spectral range of $8\mu\text{m}$ to $14\mu\text{m}$, a response time of 14ms , and they offer direct analog output via K-type thermocouple voltage readings. The range for emissivity settings of these pyrometers is 0.100 to 1.100 ; for this study, the pyrometers were set to 0.98 . The ideal spot size was determined to be 8 mm for minimal interference from the thermocouple position and optimal coverage of the substrate surface. Spot size of the pyrometer was determined via linear interpolation based on the optical chart supplied in the datasheet for the Optris CS LT pyrometers [22]. For all experiments in this study, pyrometers were positioned 30 mm away for a spot size of 8 mm on the side of the substrate. A polymer bracket was made for each spot pyrometer using ABS filament; this design included hoods over the top side of the pyrometer to minimize the effect of welding arc on the pyrometer measurement during deposition.

Each sensor was connected to an analog channel of a DATAQ DI-2008 and read as a K-type thermocouple with a sample rate of 25 Hz. These sensors are numbered and referenced in this paper corresponding to their indexing as shown in Figure 1. Each sensor is positioned 5 mm from its respective face center point for consistency, with the exception of the probe, at 6 mm away on the outside of the welded thermocouple as noted with orange dimension brackets. Here, pyrometers are shown in red, welded thermocouples in green, and the probe thermocouple in yellow. Two DI-2008 data acquisition (DAQ) devices were required to collect data from all sensors used in this study. The six thermocouples were all connected to one DAQ while the remaining sensors were connected to the other. A previously developed Robot Operating System 2 (ROS 2) stack was used to collect data from each temperature sensor (via the DI-2008) and record in a time-synchronized manner for comparison [11] [13]. The data was recorded from the ROS 2 stack as a rosbag file and then parsed into an .h5 file. This .h5 file was post-processed and analyzed via Python.

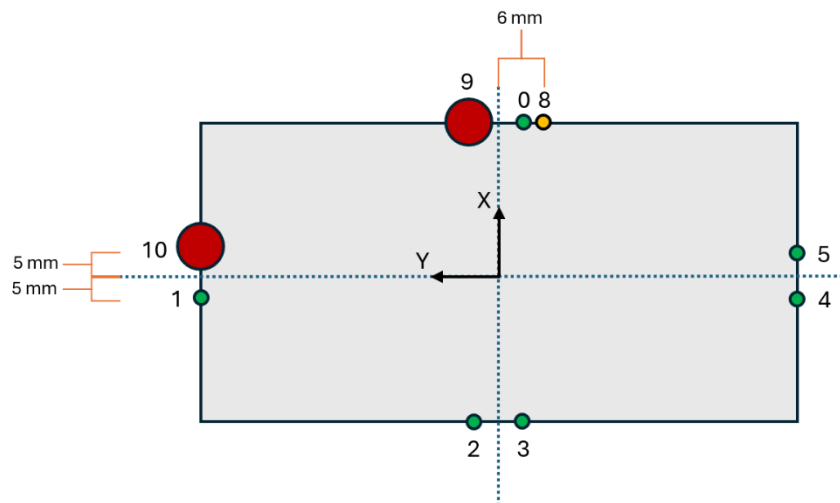


Figure 1: Sensor setup on 51 mm x 102 mm thinwall substrate. Green corresponds to welded thermocouples and red indicates 1D spot pyrometers used in this study.

Two geometries were chosen to evaluate thermal monitoring efficacy between these sensors, a thinwall and block. These were fabricated with ER70S-6 welding wire via cold metal transfer (CMT) using an ABB IRB 2600 industrial robot, ABB IRBP A250 positioner, and Fronius TPS 400i CMT welder as shown in Figure 2. RAPID code in Robotstudio was developed to execute these builds, and ROS 2 was used for data collection and visualization. The shielding gas used was 75% argon, 25% carbon dioxide with a flow rate of 15 L/min. For all builds detailed in this study, the CMT Universal Synergic line 3638 was used with wire feed of 195 ipm. A wire stick-out of 15 mm was set for all builds. A 51 mm x 102 mm substrate was used for the thinwall, and a 102 mm x 102 mm substrate was used for the block.

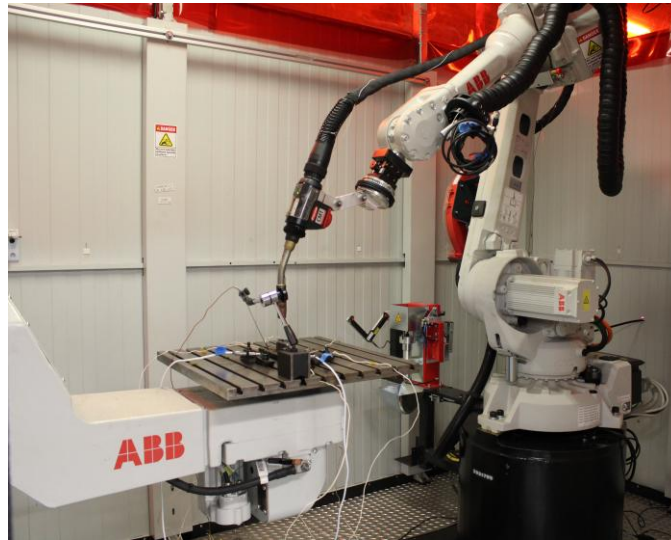


Figure 2: Wire-arc directed energy deposition setup

To begin this study, a pilot experiment was completed with a thinwall geometry. This experiment was used initially to draw preliminary conclusions as to the best method for comparison between these sensors. Two welded thermocouples, two 1D pyrometers, and one contact probe thermocouple were used. The sensors were positioned as shown in Figure 3a, with the welded thermocouple and pyrometer on the 51 mm side of the substrate each 10 mm from the face center point to their respective side. Two clamps were used, with one at the center of each of the opposing perpendicular faces as shown in Figure 3a. This thinwall consisted of 32 layers. The results of this pilot experiment showed that a direct comparison could not yet be made between the sensors with the current configuration. As shown in Figure 3b, the difference between welded thermocouple 1 and pyrometer 3 reaches up to 100 °C difference compared to the difference between welded thermocouple 2 and pyrometer 2, which only reaches a 50 °C max difference. This data was not sufficient to make reliable comparisons between these sensors as the symmetric nature of the measurements was brought into question.

Therefore, a number of factors in the setup of this experiment were adjusted to make proper comparisons between these sensors. First, additional thermocouples were added to the experimental setup to allow for symmetry not only in the same plane but across the substrate, with a thermocouple on the opposite face of each sensor in the same position. Next, the position of sensors was changed to be consistent across all groupings such that all welded thermocouples and pyrometers were set 5 mm from the face center point of their designated surface as outlined in Figure 1. Finally, the position and clamping of the substrate was adjusted to promote symmetric temperature distribution during deposition and cooling for optimal comparison between sensors.

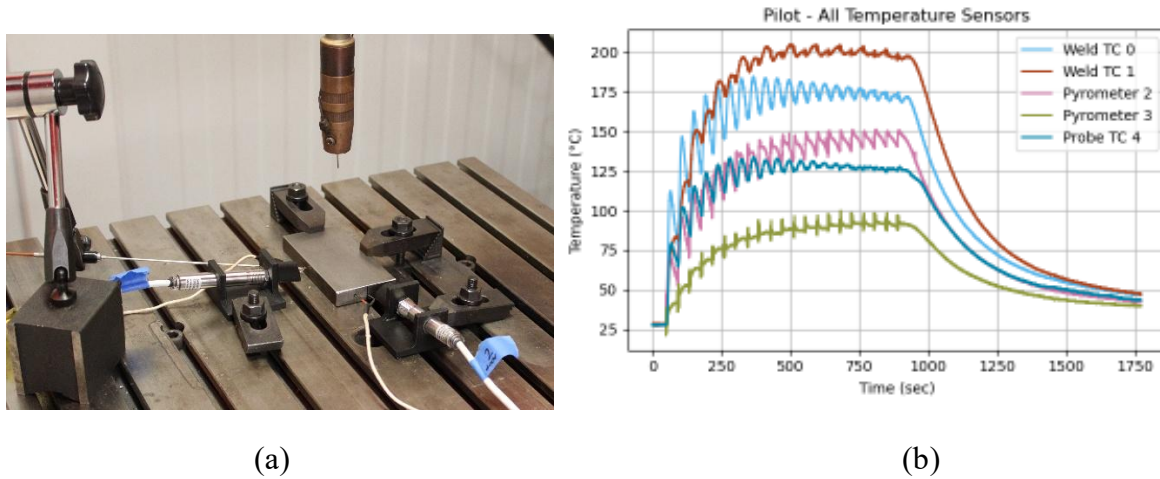


Figure 3: (a) Temperature comparison pilot study thinwall experimental setup (b) Pilot study thermal monitoring results

Thinwalls are a common experimental geometry in arc-DED because they serve as a fundamental test for assessing thermal management [6][10]. The thinwall for this study consisted of 20 layers, and an alternating build strategy was used. A wire feed speed of 195 ipm and travel speed of 10 mm/s were set for this build. A fixed dwell time of 45 seconds, 1.5 mm layer height, and 60 mm bead length were assigned in RAPID for all layers. An Optris PI-400 was used for supplemental thermal monitoring. To promote symmetric thermal distribution and cooling, the substrate was positioned in the center of the t-slot plate on the A250 position. The clamping method for this build was designed for symmetric contact and conduction from the substrate during deposition. Two clamps were used for this build: one positioned at the upper left corner and the other diagonally across at the lower right corner as shown in Figure 4a.

The block geometry was completed next to test a geometry where heat saturation could occur in the build area to test a more realistic case for the medium- and large-scale geometries targeted with this process. This block consisted of 20 layers on a 102 mm x 102 mm substrate. The same dwell time, wire feed speed, and travel speed from the thinwall geometry were used for the block (i.e. 45 seconds, 195 ipm, 10 mm/s). However, the layer height and bead length were changed to 1.8 mm and 48 mm, respectively. For this build, a meander strategy was used to

build the block with a 4 mm hatch spacing and alternating build direction by 90 ° for each layer. This pattern continued until 12 beads were deposited for one layer. Optris PI-400 and XI-400 IR cameras were used to monitor the thermal profile of this build alongside the thermocouples and pyrometers. To maintain symmetric thermal distribution via conduction, the substrate was again positioned in the center of the t-slot plate. However, instead of using two diagonal clamps like the thinwall, four clamps were used for the block's 102 mm x 102 mm substrate. One clamp was used in each corner as shown in Figure 4b to secure the substrate to the t-slot to promote symmetric thermal distribution and account for the increase in thermal energy and deposited mass.

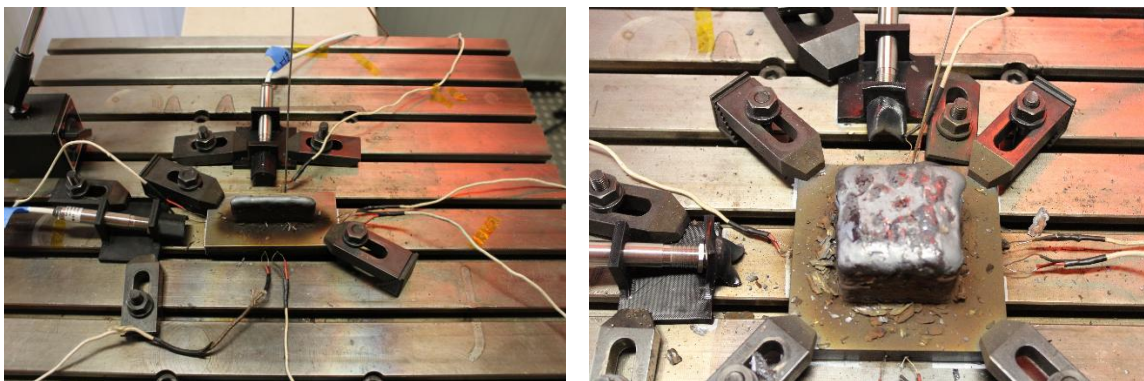


Figure 4: (a) Clamping and sensor setup for thinwall (b) Clamping and sensor setup for block geometry

Results and Discussion

Pyrometer temperature measurements were compared to their in-plane and symmetric welded thermocouple counterparts to evaluate the efficacy of their use for thermal monitoring of the substrate. Comparisons were made to evaluate the overall maximum temperature difference, overall average temperature difference, and maximum temperature difference for each layer to see at what point the closest and farthest measurements were recorded during the build.

For the thinwall geometry, the pyrometers and thermocouples have a relatively consistent difference between comparative sensors. The difference between these sensors became more consistent as the build increased in height and more layers were deposited, as shown in Figure 5, which represents all sensors in this experiment. Pyrometer 9 stayed more consistent with its in-plane and symmetric welded thermocouples as shown in Figure 6 compared to pyrometer 10 in Figure 7, which likely encountered errors in its measurement due to interference of the welding arc or surface roughness of the substrate in its focus area. The symmetric and in-plane thermocouples with pyrometer 9 had nearly equivalent differences in temperature, with an average difference of 30 °C between pyrometer 9 and thermocouple 0 (in-plane), and 31 °C between pyrometer 9 and thermocouple 2 (symmetric). In contrast, the average

difference in temperature was 46 °C between pyrometer 10 and thermocouple 1 (in-plane), and reached up to 52 °C between pyrometer 10 and thermocouple 5 (symmetric).

The average differences were calculated over the full duration of the build, from the start of deposition to the end of the cooling curve. For each timestamp, the pyrometer measurement was subtracted from the measurement of its corresponding thermocouple, then these differences were averaged across the entire build. These average difference values are shown in Table 1, and quantify the mean gap between the two sensors for each geometry. While these values are not intended for quantitative comparison with results in published literature, they allow for direct comparison between the geometries observed in this study. The magnitude of these average differences indicates potential measurement error between builds and variation in thermal profiles, this is most evident from the differing maxima values as shown in Figures 11 and 12. These findings motivate use of a close lens on the 1D spot pyrometers to reduce this measurement gap by minimizing the spot size such that the measurement area for each sensor is more comparable.

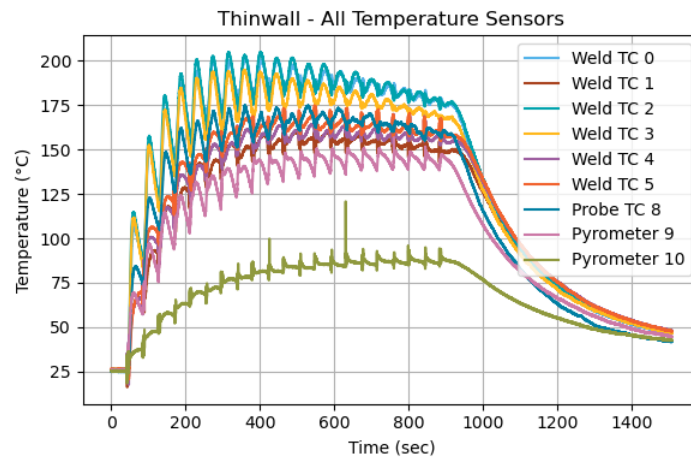


Figure 5: Temperature comparison for thinwall sensors

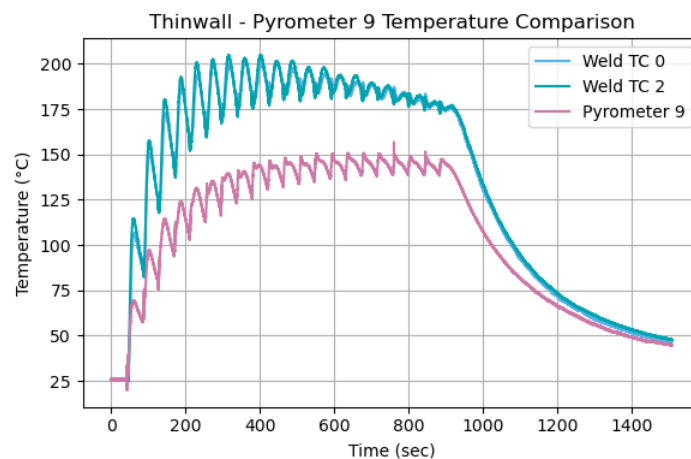


Figure 6: Temperature comparison for thinwall pyrometer 9

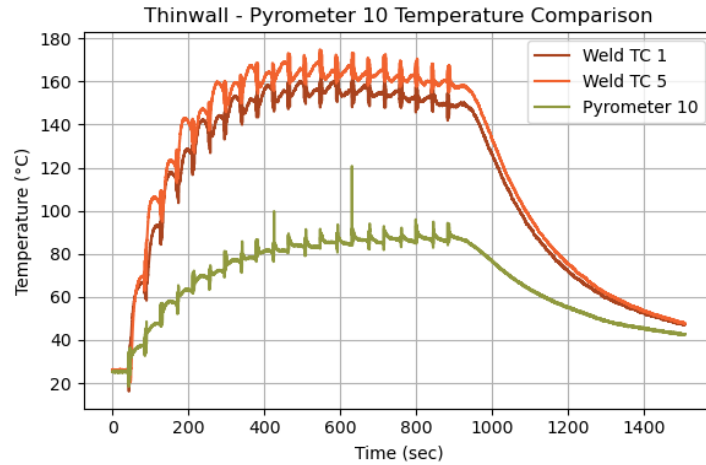


Figure 7: Temperature comparison for thinwall pyrometer 10

For the block geometry, the ambient temperature in the weld area reached significantly higher than that of the thinwall. This caused the ABS pyrometer mounts to melt, such that after layer 14, pyrometer 10 was not able to read properly as shown in Figure 8. Pyrometer 9 then failed at layer 17. Prior to this issue, the differences between measurements for the pyrometers and their corresponding thermocouples were much higher during the first few and began to even out as the build continued to increase in height similarly to the thinwall. For this build, pyrometer 9 also stayed closer to the measurements of its thermocouple counterparts compared to pyrometer 10 and showed more consistency in the measurement. For example, the average difference was 60 °C between pyrometer 9 and thermocouple 0, and 56 °C between pyrometer 9 and thermocouple 2 as shown in Figure 9. In contrast, the average difference was 69 °C between pyrometer 10 and thermocouple 1 and 81°C between pyrometer 10 and thermocouple 5 as shown in Figure 10. However, the difference between these pyrometers was much closer for this geometry than the thinwall. For example, the difference between the pyrometers for this block was 15 °C on average, whereas the average difference between them for the thinwall was 37 °C.

Table 1: Average temperature difference comparison for pyrometers on thinwall and block geometries

Comparison Type	Sensors	Average Difference (Thinwall)	Average Difference (Block)
In-Plane	Pyrometer 9 & Thermocouple 0	30 °C	60 °C
Symmetric	Pyrometer 9& Thermocouple 2	31 °C	56 °C
In-Plane	Pyrometer 10 & Thermocouple 1	46 °C	69 °C
Symmetric	Pyrometer 10 & Thermocouple 5	52 °C	81 °C

After layer 15 of this build, the hood of the ABS mounts for the pyrometers melted, covering the view of the pyrometers for all following layers. Also, due to the heat accumulation of the block with a 45-second dwell time, the pyrometer was exposed to ambient temperature above its operating limit (80 °C) from layers 15-20.

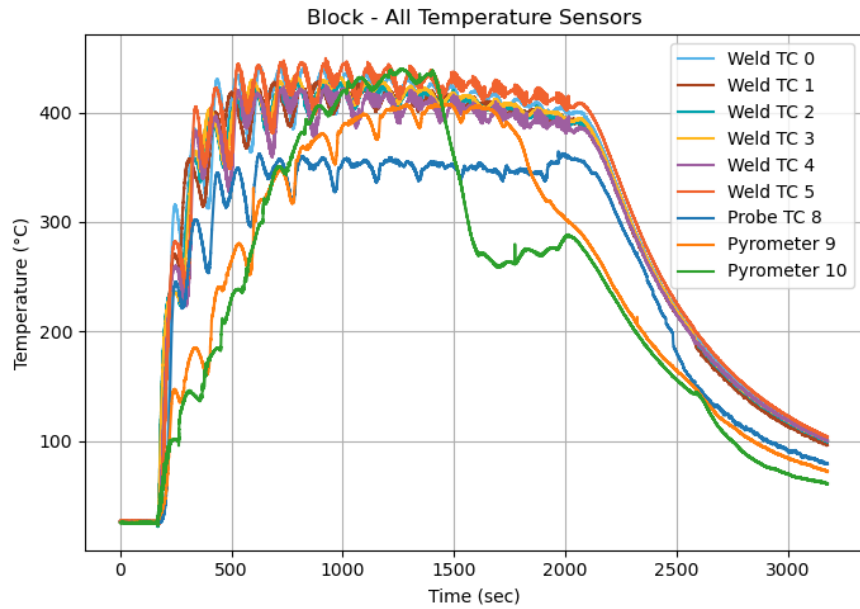


Figure 8: Temperature comparison for block sensors

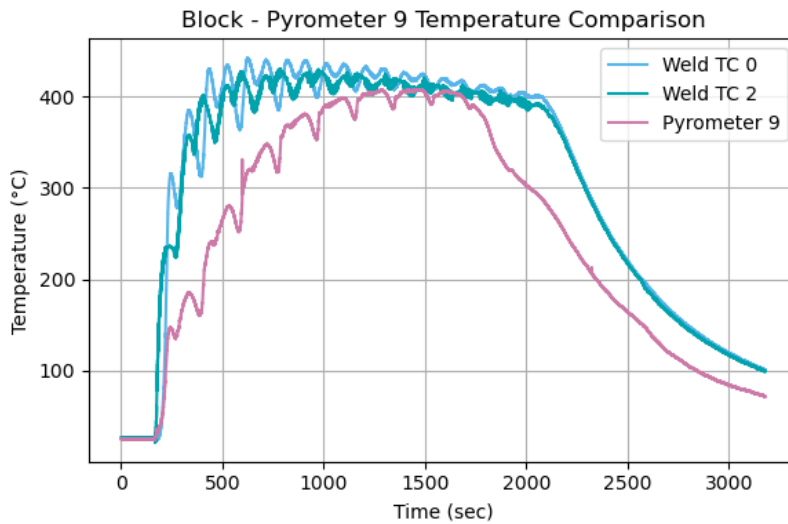


Figure 9: Temperature comparison for block pyrometer 9

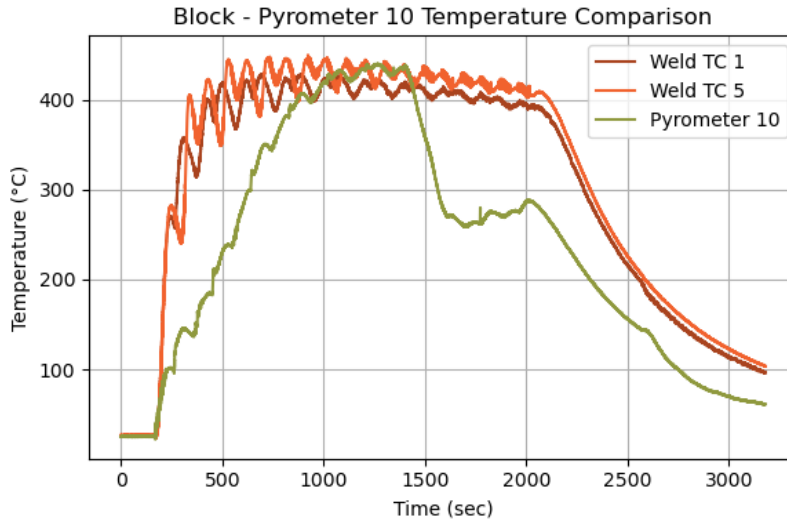


Figure 10: Temperature comparison for block pyrometer 10

At the beginning of the block build, the pyrometers diverged much more significantly than during the beginning of the thinwall. However, as the part was built up, they showed a similar yet more aggressive trend of convergence for the block leading up to the mount obstruction issue at layer 14 as shown in Figures 12 and 13.

The pyrometers were also compared to their in-plane and symmetric counterparts by looking at the maximum difference in the temperature measurement for each layer as shown in Figures 11 and 12. For pyrometer 9, the maximum difference in temperature over the duration of the build is relatively consistent, within the range of 38 (lowest) to 70 (highest) °C for the thinwall. However, pyrometer 0 looks much different for the block geometry. During the start of this build, the difference between the pyrometer and thermocouple measurements was high, reaching up to 234 °C on layer 3. After this layer, we see that pyrometer 9 converges toward the thermocouple measurements over the next 12 layers of the block, reaching as close as 6 °C difference on layer 15. The comparison for pyrometer 10 between the thinwall and block geometries shown in Figure 12 depicts a similar response. However, the discrepancy between maximum difference values for pyrometer 10 in layers 6 to 13 is much more substantial than for pyrometer 9 on these geometries.

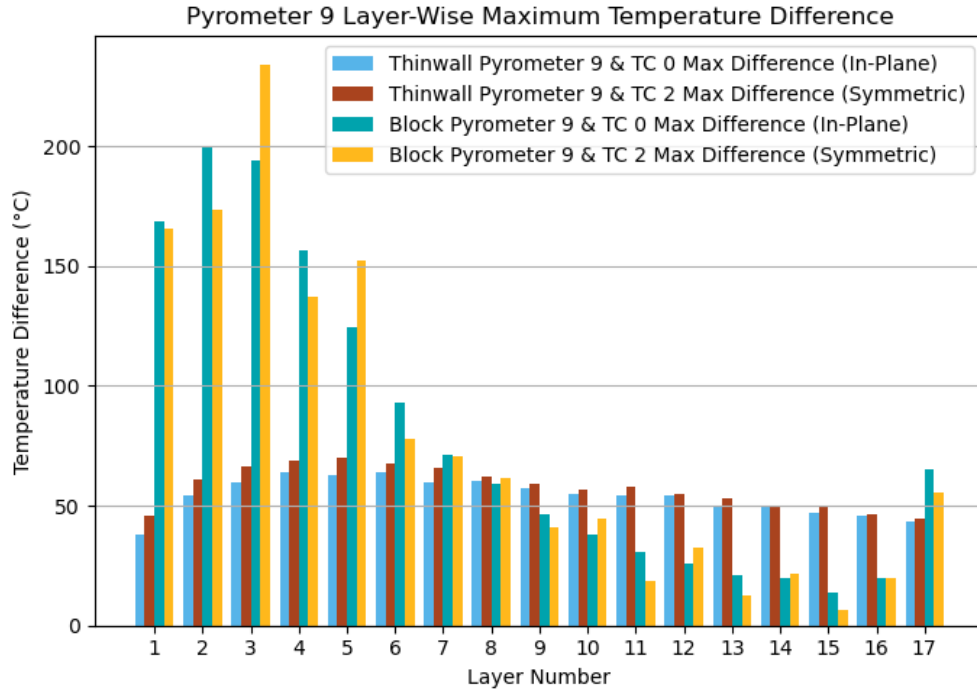


Figure 11: Layer-wise temperature difference for pyrometer 9 on thinwall and block

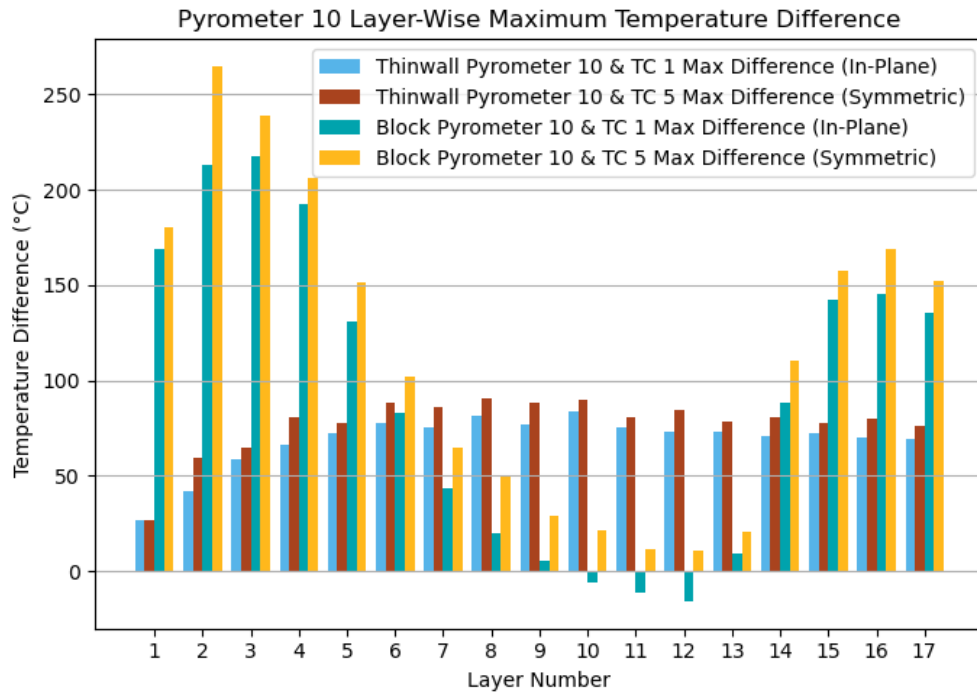


Figure 12: Layer-wise temperature difference for pyrometer 10 on thinwall and block

Conclusion

For the thinwall geometry, pyrometer 9 (5 mm right from center on 102 mm face) showed a more consistent trend when compared to its thermocouple counterparts. Though pyrometer 10 (5mm right from center of 51 mm face) also showed consistency in comparison to its thermocouple counterparts, it was exposed to error and cannot be reliably compared. It is hypothesized that this error was introduced due to pyrometer 10's head-on view of the welding arc as it was positioned perpendicular to the build direction. That said, the measurements between these pyrometers for the thinwall, though consistent, diverged greatly. In comparison, during deposition of the block geometry, readings between these pyrometers converged, especially between layers 6 and 13. Pyrometer 10 was observed to have less error in its measurements from the welding arc during deposition of the block as well. However, both pyrometers were exposed to high ambient temperatures during this weld, causing the mounts securing them to melt downward over their view, and were not able to provide reliable readings past layer 14.

This study shows that 1D pyrometers are a promising option for thermal monitoring in areas where welded thermocouples are commonly used under proper operating conditions and amount of deposited material observed based on the converging results of the block geometry. Mounting strategies and spot size are important factors in the success of their use in this fashion. In future work, a close lens will be used with these pyrometers to increase the distance from the deposited area while concentrating the required spot size. More robust mounts will also be fabricated out of aluminum to secure the position of these sensors and concentrate their view on the target area with improved coverage to shield from effects of the welding arc. The results of these modifications could provide more insight into the thermal profile of parts fabricated with arc-DED during deposition without disruption of the welding process, preserving part quality and desirable mechanical properties.

References

- [1] C. R. Cunningham, J. M. Flynn, A. Shokrani, V. Dhokia, and S. T. Newman, “Invited review article: Strategies and processes for high quality wire arc additive manufacturing,” *Additive Manufacturing*, vol. 22, pp. 672–686, Aug. 2018, doi: 10.1016/j.addma.2018.06.020.
- [2] A. Yıldız, K. Davut, B. Koc, and O. Yılmaz, “Wire arc additive manufacturing of high-strength low alloy steels: study of process parameters and their influence on the bead geometry and mechanical characteristics,” *The International Journal of Advanced Manufacturing Technology*, vol. 108, Jun. 2020, doi: 10.1007/s00170-020-05482-9.
- [3] K. Li et al., “A critical review on wire-arc directed energy deposition of high-performance steels,” *Journal of Materials Research and Technology*, vol. 24, pp. 9369–9412, May 2023, doi: 10.1016/j.jmrt.2023.05.163.
- [4] F. Pixner et al., “Thermal cycling effects on the local microstructure and mechanical properties in wire-based directed energy deposition of nickel-based superalloy,” *Additive Manufacturing*, vol. 83, p. 104066, Mar. 2024, doi: 10.1016/j.addma.2024.104066.
- [5] B. Wu et al., “Effects of heat accumulation on the arc characteristics and metal transfer behavior in Wire Arc Additive Manufacturing of Ti6Al4V,” *Journal of Materials Processing Technology*, vol. 250, pp. 304–312, Dec. 2017, doi: 10.1016/j.jmatprotec.2017.07.037.
- [6] J. Li, T. Liu, K. Zhang, Z. Zou, X. Lu, and Z. Zhu, “The thermal history of the directed energy deposition process monitored by pyrometer and camera,” *Meas. Sci. Technol.*, vol. 35, no. 4, p. 045204, Jan. 2024, doi: 10.1088/1361-6501/ad1dab.
- [7] J. Guzman, “Unraveling the Role of Thermal History on Residual Stress, Dimensional Accuracy, and Yield Strength in Wire-Arc Directed Energy Deposition - ProQuest.” Accessed: Jul. 08, 2025. [Online]. Available: <https://www.proquest.com/docview/3215951372?pq-origsite=gscholar&fromopenview=true&sourcetype=Dissertations%20&%20Theses>
- [8] G. J. Marshall, S. M. Thompson, and N. Shamsaei, “Data indicating temperature response of Ti–6Al–4V thin-walled structure during its additive manufacture via Laser Engineered Net Shaping,” *Data in Brief*, vol. 7, pp. 697–703, Jun. 2016, doi: 10.1016/j.dib.2016.02.084.
- [9] C. Zamiela, R. Stokes, W. Tian, H. Doude, M. W. Priddy, and L. Bian, “Physics-Informed Approximation of Internal Thermal History for Surface Deformation Predictions in Wire Arc Directed Energy Deposition,” *Journal of Manufacturing Science and Engineering*, vol. 146, no. 081007, May 2024, doi: 10.1115/1.4065416.
- [10] S. Islam et al., “Investigation of residual stress distribution in wire-arc directed energy deposited refractory molybdenum alloy utilizing numerical thermo-mechanical analysis and neutron diffraction method,” *International Journal of Refractory Metals and Hard Materials*, vol. 130, p. 107149, Aug. 2025, doi: 10.1016/j.ijrmhm.2025.107149.

- [11] R. Stokes, “An open-source digital twin of the wire arc directed energy deposition process for interpass temperature regulation,” Theses and Dissertations, May 2024, [Online]. Available: <https://scholarsjunction.msstate.edu/td/6182>
- [12] K.A. Cummings, “Improved part-scale FE thermal monitoring of wire-arc ded via incorporation of the build platform assembly” (2025). Theses and Dissertations
- [13] J. Betts, “Advancing digital twins of wire arc-DED through process control with a multi-modal sensor array,” Theses and Dissertations, Dec. 2024, [Online]. Available: <https://scholarsjunction.msstate.edu/td/6397>
- [14] A. Ameen, V. Janik, J. Nicholas, X. Zhang, and C. E. Seow, “Comparison of process control methods for wire-arc directed energy deposition of low carbon steels with in-situ temperature measurement,” 2023, Accessed: Jul. 08, 2025. [Online]. Available: <https://hdl.handle.net/2152/124441>
- [15] D. Baier, T. Weckenmann, F. Wolf, A. Wimmer, and M. F. Zaeh, “Underlying Methodology for a Thermal Process Monitoring System for Wire and Arc Additive Manufacturing,” *Journal of Manufacturing and Materials Processing*, vol. 7, no. 1, Art. no. 1, Feb. 2023, doi: 10.3390/jmmp7010010.
- [16] M. J. Dantin, W. M. Furr, and M. W. Priddy, “Toward a Physical Basis for a Predictive Finite Element Thermal Model of the LENSTM Process Leveraging Dual-Wavelength Pyrometer Datasets,” *Integr Mater Manuf Innov*, vol. 11, no. 3, pp. 407–417, Sep. 2022, doi: 10.1007/s40192-022-00271-6.
- [17] J. Wang, B. Zhao, Y. Liu, J. Zhao, and G. Ma, “Research Progress in Shape-Control Methods for Wire-Arc-Directed Energy Deposition,” *Materials*, vol. 17, no. 23, Art. no. 23, Jan. 2024, doi: 10.3390/ma17235704.
- [18] A. Ma, “The Potential of IR Pyrometry for Monitoring Interpass Temperature in Wire + Arc Additive Manufacturing,” *EME*, vol. 3, no. 1, pp. 1–4, Sep. 2019. doi: 10.31031/EME.2019.03.000553
- [19] N. Kozamernik, D. Bračun, and D. Klobčar, “WAAM system with interpass temperature control and forced cooling for near-net-shape printing of small metal components,” *Int J Adv Manuf Technol*, vol. 110, no. 7, pp. 1955–1968, Sep. 2020, doi: 10.1007/s00170-020-05958-8.
- [20] J. Müller and J. Hensel, “Potential of thermography for the monitoring of DED-Arc processes,” *Weld World*, vol. 68, no. 3, pp. 505–513, Mar. 2024, doi: 10.1007/s40194-023-01676-3.
- [21] F. Pixner, R. Buzolin, S. Schönfelder, D. Theuermann, F. Warchomicka, and N. Enzinger, “Contactless temperature measurement in wire-based electron beam additive manufacturing Ti-

6A1-4V,” *Weld World*, vol. 65, no. 7, pp. 1307–1322, Jul. 2021, doi: 10.1007/s40194-021-01097-0.

[22] Optris GmbH, *Infrared Thermometer Optris CS LT Datasheet*, Version 11-A, Sep. 2024. [Online]. Available: https://optris.com/wp-content/uploads/2024/09/CS-LT-DS-EN2024-11-A_web.pdf